Photodiagnosis and Photodynamic Therapy 27 (2019) 156–161

Contents lists available at ScienceDirect

Photodiagnosis and Photodynamic Therapy

journal homepage: www.elsevier.com/locate/pdpdt

Diagnosis of cervical squamous cell carcinoma and cervical adenocarcinoma based on Raman spectroscopy and support vector machine

Chengxia Zheng[a,g], Song Qing[b], Jing Wang[c], Guodong Lü[d], Hongyi Li[e], Xiaoyi Lü[a,*], Cailing Ma[c,**], Jun Tang[f], Xiaxia Yue[f]

[a] College of Information Science and Engineering, Xinjiang University, Urumqi 830046, China
[b] Pathology Department of The First Affiliated Hospital of Xinjiang Medical University, Urumqi 830054, China
[c] Gynecology Department of The First Affiliated Hospital of Xinjiang Medical University, Urumqi 830054, China
[d] State Key Laboratory of Pathogenesis, Prevention, and Treatment of Central Asian High Incidence Diseases, The First Affiliated Hospital of Xinjiang Medical University, Urumqi 830054, Xinjiang, China
[e] Quality of Products Supervision and Inspection Institute, Urumqi 830011, Xinjiang, China
[f] Physics and Chemistry Detecting Center, Xinjiang University, Urumqi 830046, China
[g] Changji Vocational and Technical College, Changji City 831100, Xinjiang Uygur Autonomous Region, China

ARTICLE INFO

Keywords:
Tissue
Raman spectrum
Cervical adenocarcinoma
Cervical squamous cell carcinoma
PCA-SVM
Raman spectroscopy

ABSTRACT

In this report, we collected the Raman spectrum of cervical adenocarcinoma and cervical squamous cell carcinoma tissues by a micro-Raman spectroscopy system. We analysed, compared and summarized the characteristics and differences of the normalized mean Raman spectra of the two tissues and pointed out the major differences in the biochemical composition between the two tissues. The PCA-SVM model that was used to distinguish the two types of cervical cancer tissues was established. The accuracy of the model in differentiating cervical adenocarcinoma from cervical squamous cell carcinoma was 93.125%.

The results of this study indicate that Raman spectroscopy of cervical adenocarcinoma and cervical squamous cell carcinoma tissue in combination with SVM (support vector analysis) and PCA (principal component analysis) can be useful for the classification of cervical adenocarcinoma and cervical squamous cell carcinoma tissues and for the exploration of the differences in biochemical compositions between the two types of cervical tissue. This study lays a foundation to further study Raman spectroscopy as a clinical diagnostic method for cervical cancer.

1. Introduction

Cervical cancer ranks as the fourth most frequently diagnosed cancer and the fourth leading cause of cancer death in women, with an estimated 570,000 cases and 311,000 deaths in 2018 worldwide [1]. Squamous cell carcinomas account for approximately 80% of all cervical cancers, and adenocarcinoma accounts for approximately 20% [2]. There are differences between cervical adenocarcinoma and cervical squamous cell carcinoma in surgical treatment and the use of postoperative adjuvant chemotherapy. Cervical squamous cell carcinoma is not associated with oestrogen, and the rate of ovarian metastasis is low in early-stage patients. Therefore, the ovaries can be preserved in premenopausal patients with stage I B1, II A1 when they are younger than 45 years old. Ovarian preservation is not recommended in patients with stage I B2, II A2 or above [2]. The ovarian metastasis rate of cervical adenocarcinoma is approximately 10% on average; thus, ovarian preservation is not recommended [2]. The histological type of the tumour (adenocarcinoma, squamous cell carcinomas, etc.) should be considered as a median risk factor for whether postoperative complementary chemotherapy should be used. Moreover, adenocarcinomas are less sensitive to radiotherapy than squamous cell carcinomas [2,3]. Therefore, the correct differentiation between cervical adenocarcinoma and cervical squamous cell carcinoma and the adoption of the correct treatment regimen are conducive to improving the survival rate of patients.

At present, the primary screening tool for cervical cancer is a Pap smear. Colposcopy is another widely used tool, which usually follows an abnormal Pap smear. However, these methods have several shortcomings such as high false negative/positive results [14], time-consuming, expensive and traumatic. Therefore, it is particularly important

* Corresponding author at: College of Information Science and Engineering, Xinjiang University, Urumqi 830046, China.
** Corresponding author.
E-mail addresses: xiaoz813@163.com (X. Lü), hymcl13009661999@126.com (C. Ma).

https://doi.org/10.1016/j.pdpdt.2019.05.029
Received 31 January 2019; Received in revised form 24 May 2019; Accepted 24 May 2019
Available online 25 May 2019

and urgent to find a rapid, economical, non-invasive and objective method for the diagnosis of cervical cancer.

Raman spectroscopy has been widely exploited for the detection of cervical cancer as a non-invasive, objective and rapid technique [4–10,14]. However, there are no studies on the use of Raman spectroscopy to differentiate cervical adenocarcinoma from squamous cell carcinoma. It has been reported that an endoscopic Raman detection system for nasopharyngeal carcinoma has been developed [11]. An endoscopic Raman detection system has a great potential for clinical detection of cancers [12]. In our study, the normalized mean Raman spectra of cervical adenocarcinoma and cervical squamous cell carcinoma tissues were compared and analysed. PCA-SVM was used to establish the differential models of two types of cervical cancer tissues with an accuracy of 93.125%. It lays a foundation for further research on the endoscopic Raman detection system for clinical diagnosis of cervical cancer.

2. Experimental section

2.1. Materials and methods

Raman spectral maps from cervical tissue samples of 95 different patients, including 45 cervical adenocarcinoma and 50 cervical squamous cell carcinomas were acquired. For each sample, a tissue section of 10 μm thickness was cut from the formalin fixed paraffin processed cervical tissue block using a microtome. After dewaxing with xylene, Raman spectra were obtained according to standard clinical procedures [4,13,16]. The Raman spectra were acquired in the spectral range of 400–1800 cm^{-1} using a Raman system (LabRAM HR Evolution RAMAN SPECTROMETER, HORIBA Scientific Ltd) at ambient temperature (25 ± 1 ℃. A 532 nm laser [17] was focused through a 50× objective (NA = 0.5) to excite the samples. The spectra were collected at 100 μm steps across whole sections

to provide information about the global changes in the specimen [21]. At least five to seven spectra were recorded on each sample at different locations and each spectral point was treated as a sample [14,18,19]. An integration time of 8 s and 3 accumulations were the parameters used for spectral recording. These conditions were kept constant for all measurements. A total of 658 pieces of spectral data were obtained, including 315 pieces of adenocarcinoma spectral data and 343 pieces of squamous cell carcinoma spectral data.

2.2. Data preprocessing of Raman maps

Data preprocessing included substrate backgrounds, baseline correction and normalization. The raw Raman spectra acquired from the tissue samples contained high fluorescence background and noise. To extract the pure Raman signals, an airPLS algorithm was employed to subtract the cervical tissue autofluorescence background, and to correct the baseline [20]. Then, the data normalization function mapminmax of MATLAB was used to normalize all the spectral data to 0–1 [4]. Thus, the change in relative spectral intensity, which may be caused by a power fluctuation of the Raman laser source, can be reduced and the comparison of Raman peak shapes and relative intensities between different tissue samples could be achieved. OriginPro19.0 software was used to plot the mean spectrogram of the pretreated spectral data for two types of cervical cancer tissues. PCA-SVM was used to establish a discrimination model for all the spectral data of cervical adenocarcinoma and cervical squamous cell carcinoma after pretreatment.

3. Results and discussion

3.1. Spectral analysis

The significant differences in Raman spectra between cervical adenocarcinoma and cervical squamous cell carcinoma can be seen in

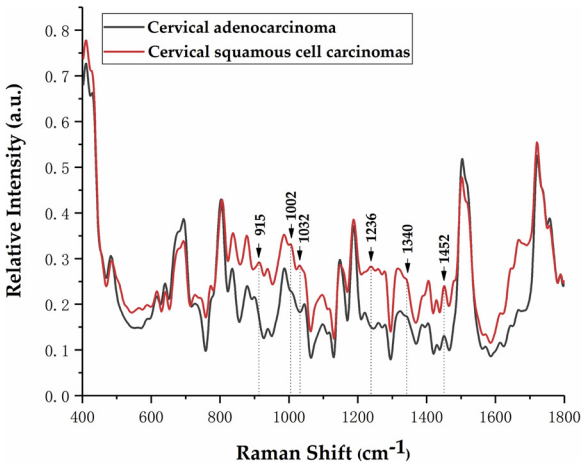

Fig. 1. Normalized mean Raman spectrum of cervical adenocarcinoma and cervical squamous cell carcinoma tissues.

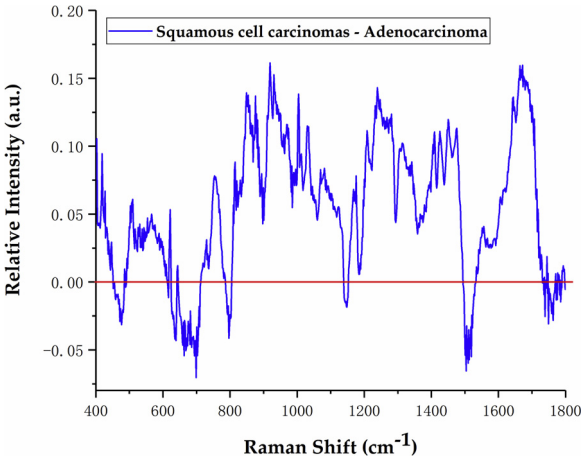

Fig. 2. Difference spectrum of the normalized mean spectrum (cervical squamous cell carcinoma–cervical adenocarcinoma).

Fig. 1 and 2. These differences are reflected in the relative intensity, position and shape of the Raman peaks. The distinctive Raman features and intensity differences in adenocarcinoma vs. squamous cell carcinoma cervical tissue can reflect differences in the biochemical components associated with types of cervical cancer. It can be observed from Fig. 1 that the Raman peaks of the mean Raman spectra of the two types of cervical cancer tissues mainly appeared at 415, 485, 614, 640, 695, 838, 880, 938, 1002, 1095, 1340, 1452, 1506, 1616, 1645, 1670 and 1756 cm^{-1}. These peaks appear in the same position and have a similar shape, but there are significant differences in their relative intensities, which can be more clearly illustrated by displaying the spectrum differences, which was computed by subtracting the normalized mean spectrum of cervical adenocarcinomas from the normalized mean spectrum of cervical squamous cell carcinomas, as shown in Fig. 2. The strong positive peaks seen in the difference spectrum (Fig. 2), 415, 614, 838, 880, 938, 1002, 1095, 1340, 1452, 1616, 1645, 1670 cm^{-1}, are contributed by the spectrum of cervical squamous cell carcinomas. These spectral bands based on peak positions and relative intensities can be tentatively assigned to lipids, proteins (tryptophan, phenylalanine, amide I (α-helix)), carbohydrates, DNA (nucleic acid) using the available literature data [10,15,18,21]. The negative peaks, 485, 640, 695, 1506 cm^{-1}, are contributed by the spectrum of cervical adenocarcinoma, and these bands can be assigned to biomolecules such as DNA (cytosine), proteins (tyrosine, methionine) and glycogen [10,13,15]. The peak assignments are listed in Table 1. The peaks at 640, 695, 838, 880, 1002, 1032, 1043, 1236, 1616, 1645, 1670 cm^{-1}

Table 1
Raman peak attribution in cervical cancer tissues.

Raman bands/cm^{-1}	Assignations
415	Phosphatidylinositol
485	Glycogen
614	Cholesterol ester
640	C–S stretching and C–C twisting of proteins-tyrosine
695	ν(C–S) trans (amino acid methionine)
838	Deformative vibrations odd amine groups
880	Tryptophan, δ (ring)
898	Monosaccharides (β-glucose), (C—O—C) skeletal mode, Disaccharide (maltose), (C—O—C) skeletal mode
915	Ribose vibration, one of the distinct RNA modes
938	C—C stretch backbone
1002	Phenylalanine
1032	CH2 CH3 bending modes of collagen and phospholipids
1043	Proline (collagen assignment)
1095	Lipid
1236	CN stretch, NH bending amide III band
1340	Nucleic acid mode
1452	CH2 deformation in lipids
1506	N=H bending, Cytosine
1616	C=C stretching mode of tyrosine & tryptophan
1645	Amide I (α-helix)
1670	Amide I

can be attributed to proteins. In cervical cancer tissues, the cells have large amounts of proteins giving a protein-dominated spectrum [18]. Very prominent differences in spectral profiles for both cervical cancer tissues are observed. As seen from Fig. 1, the band at 1002 cm^{-1}, attributed to phenylalanine [18] in the normalized mean Raman spectrogram of cervical squamous cell carcinoma tissues, is 2 cm^{-1} red-shifted from the normalized mean Raman spectrogram of cervical adenocarcinoma tissues. The band at 1032 cm-^{1}, attributed to CH2/CH3 bending modes of collagen and phospholipids [15] in the normalized mean Raman spectrogram of cervical squamous cell carcinoma tissues, is 11 cm^{-1} red-shifted relative to the band at 1043 cm^{-1}, attributed to proline (collagen assignment) [23] in the normalized mean Raman spectrogram of cervical adenocarcinoma tissues. These results indicate that there is a change in the molecular structure of proteins in association with cervical cancer types [19]. There is a spectrum peak at 898 cm^{-1}, attributed to monosaccharides (β-glucose), (C—O—C) skeletal mode and disaccharide (maltose), (C—O—C) skeletal mode [21], in the normalized mean Raman spectrogram of cervical adenocarcinoma tissues, which is missing in the normalized mean Raman spectrogram of cervical squamous cell carcinoma tissues. The results indicate that the percentage of carbohydrate contents relative to the total Raman-active components are higher in cervical adenocarcinoma tissue in comparison with those of the cervical squamous cell carcinoma tissue. There is a spectrum peak at 915 cm^{-1}, attributed to ribose vibration (one of the distinct RNA modes) [22], in the normalized mean Raman spectrogram of cervical squamous cell carcinoma tissues, which is missing in the normalized mean Raman spectrogram of cervical adenocarcinoma tissues. These results indicate that the percentage of RNA contents relative to the total Raman-active components are higher in cervical squamous cell carcinoma tissue in comparison with those of the cervical adenocarcinoma tissue. The band at 1236 cm^{-1}, attributed to the CN stretch, NH bending amide III band [13] in the normalized mean Raman spectrogram of cervical squamous cell carcinoma tissues, is 16 cm^{-1} blue-shifted relative to the band at 1220 cm^{-1}, attributed to amide III (b -sheet) [13] in the normalized mean Raman spectrogram of cervical adenocarcinoma tissues, which indicates a change in structure and conformation of amide III in association with cervical cancer types.

3.2. Raman characteristic peak scatter diagram

To further clarify the differences in proteins, DNA and lipids between cervical adenocarcinoma and cervical squamous cell carcinoma tissues, the relative intensity of all the spectral data after pretreatment at 1002 (protein), 1340 (nucleic acid) and 1452 (lipid) cm^{-1} were used as the ordinate, and the number of samples were used as the abscissa to draw scatter plots as shown in Fig. 3(A, B, and C). The standard error bar diagrams of the average relative intensity of the characteristic peaks at 1002, 1340 and 1452 cm^{-1} of two types of cervical cancer tissues were also drawn and shown in Fig. 3D.

The scatter plot of the relative intensity of the characteristic peak at 1002 cm^{-1}, attributed to phenylalanine [18], is shown in Fig. 3A. As seen from Fig. 3A, the relative intensity of the spectra of cervical adenocarcinoma and cervical squamous cell carcinoma tissues at 1002 cm^{-1} is different. An independent variable t-test was performed on 315 spectral relative intensity data of cervical adenocarcinoma tissues at 1002 cm^{-1}, and 315 data randomly selected from 343 spectral relative strength data of cervical squamous cell carcinoma tissues at 1002 cm^{-1} (all the data was preprocessed). $P < 0.001$, which indicates that there is a significant difference in the spectral relative intensity between cervical adenocarcinoma and cervical squamous cell carcinoma tissues at 1002 cm^{-1}. As seen in Fig. 3D, the mean spectral relative intensity of cervical squamous cell carcinoma tissues is higher than that of cervical adenocarcinoma tissues at 1002 cm^{-1}. It has been reported in previous studies that tumours showed higher percentage signals for phenylalanine in comparison with normal tissues [10,15,24]. Phenylalanine, a protective amino acid highly present in primary tumours [26], has been associated with inhibition of tumour growth and postoperative metastasis [25,26] and has been used in studies to detect pancreatic cancer [27].

The scatter plot of the relative intensity of the characteristic peak at 1340 cm^{-1}, attributed to the nucleic acid mode [10], is shown in Fig. 3B. The relative intensity of the spectrum of cervical adenocarcinoma and cervical squamous cell carcinoma tissues at 1340 cm^{-1} is different, which can be seen in Fig. 3B. An independent variable t-test was performed on 315 spectral relative intensity data of cervical adenocarcinoma tissues at 1340 cm^{-1} and 315 data randomly selected from 343 spectral relative strength data of cervical squamous cell carcinoma tissues at 1340 cm^{-1} (all the data has been preprocessed). $P < 0.001$, which indicates that there is a significant difference in spectral relative intensity between cervical adenocarcinoma and cervical squamous cell carcinoma tissues at 1340 cm^{-1}. As seen in Fig. 3D, the mean spectral relative intensity of cervical squamous cell carcinoma tissues is higher than that of cervical adenocarcinoma tissues at 1340 cm^{-1}. The increased nucleic acid is a result of the increased proliferation of the tumour cells [13,15,19]. The results indicated that, compared with cervical adenocarcinoma tissue, cervical squamous cell carcinoma tissue had a stronger ability of cell proliferation.

The scatter plot of the relative intensity of the characteristic peaks at 1452 cm^{-1}, attributed to CH2 deformation in lipids [10], is shown in Fig. 3C. As seen from Fig. 3C, the relative intensity of spectra of cervical adenocarcinoma and cervical squamous cell carcinoma tissues at 1452 cm^{-1} is different. An independent variable t-test was performed on 315 spectral relative intensity data of cervical adenocarcinoma tissues at 1452 cm^{-1} and 315 data randomly selected from 343 spectral relative strength data of cervical squamous cell carcinoma tissues at 1452 cm^{-1} (all the data has been preprocessed). $P < 0.001$, which indicates that there is a significant difference in the spectral relative intensity between cervical adenocarcinoma and cervical squamous cell carcinoma tissues at 1452 cm^{-1}. As seen from Fig. 3D, the mean spectral relative intensity of cervical squamous cell carcinoma tissues is higher than that of cervical adenocarcinoma tissues at 1452 cm^{-1}.

3.3. PCA-SVM model

Principal component analysis (PCA) can reduce a large amount of original data to a much smaller, more manageable dataset [28]. In the literature, there are many examples of the application of PCA as an efficient tool supporting medical diagnosis [10,13,14,17,18,19,28]. A

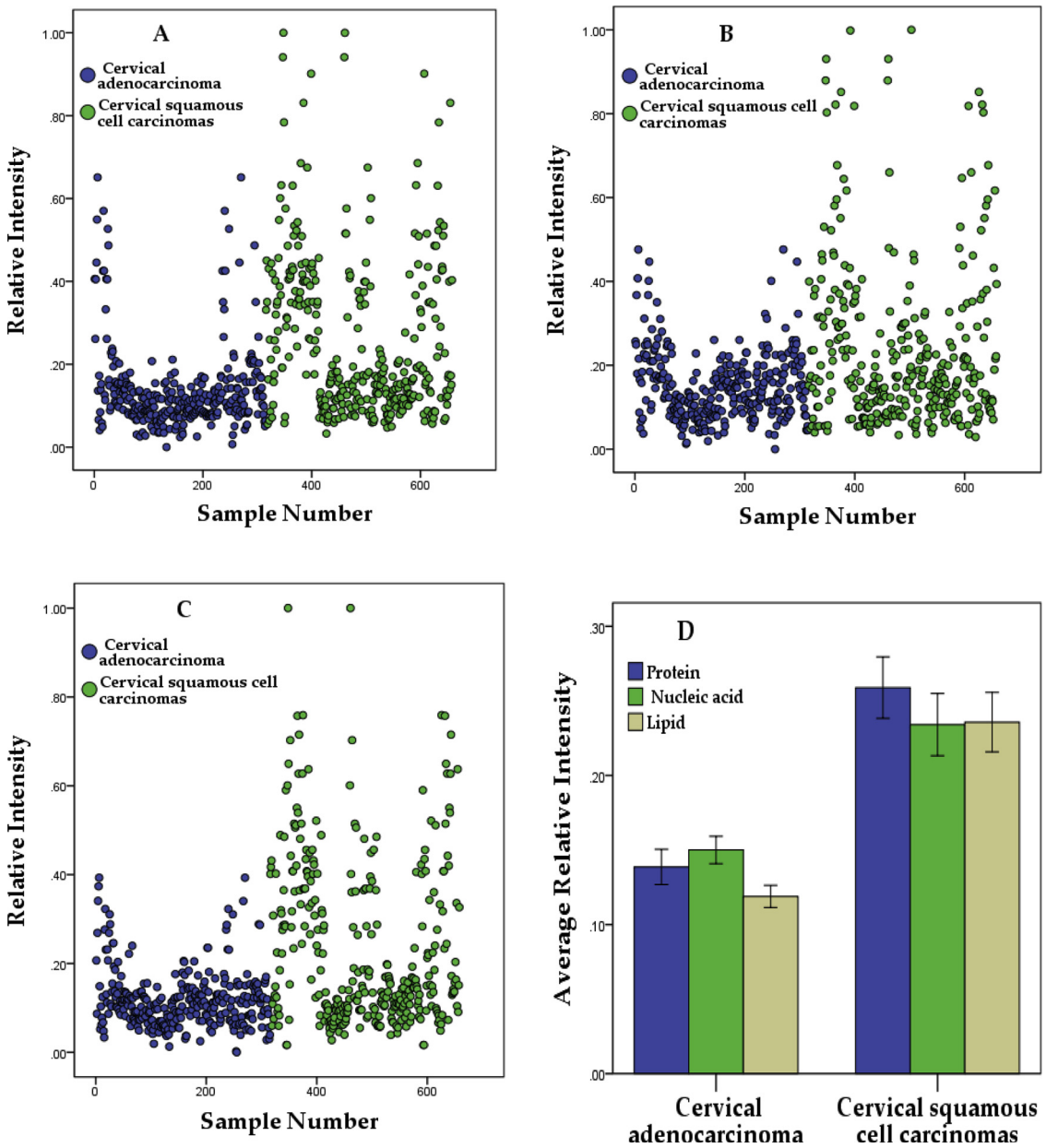

Fig. 3. Scatter diagrams of relative intensities of characteristic peaks at 1002 cm^{-1} (A), 1340 cm^{-1} (B), and 1452 cm^{-1} (C). The standard error bar diagrams of the average relative intensity of the characteristic peaks at 1002, 1340 and 1452 cm^{-1} of the two types of cervical cancer tissues (D).

support vector machine (SVM) is a powerful multi-class pattern recognition technology and is applied to analyse small sampling, nonlinear and high dimension data sets [29]. SVM belongs to the family of "margin-based classifiers" that often achieve superior classification performance compared to other classification algorithms [29]. The current study presents the use of Raman spectroscopy combined with principal component analysis (PCA) and support vector machine (SVM) for the classification of cervical adenocarcinoma and cervical squamous cell carcinoma tissues. All the spectra (unfiltered) were subjected to fluorescence background removal and baseline correction using the airPLS algorithm [20], in MATLAB 2016a before being exported to Microsoft Excel. Then, the spectra were normalized to the spectral maximum, from 0 to 1, and then principal component analysis (PCA) was carried out to reduce the data dimension 111 principal components (contribution rate > 0.95) were extracted to establish an SVM identification model between cervical adenocarcinoma and cervical squamous cell carcinoma in MATLAB 2016a. Each dataset(cervical adenocarcinoma data set and cervical squamous cell carcinoma data set was divided into training and validation sets by randomly selecting 80 samples for the validation data and the rest of the data was used for training. All the results shown in the latter part are the results of predictions from the verification set, which was not included in the training of the algorithm.

In this study, Raman spectroscopy and PCA-SVM were used to classify cervical adenocarcinoma and squamous cell carcinoma tissues. Four different kernels are used to analyse and classify the Raman spectra, and the results are shown in Table 2(A–D). To compare the classification effect, PCA-LDA was also adopted in this study to establish the classification model. The data settings were exactly the same as the PCA-SVM model, and the results are shown in Table 2E. As seen from Table 2, the classification accuracy of the PCA- SVM algorithm is higher than that of the PCA-LDA algorithm. Among them, the PCA-SVM classification model based on the polynomial kernel function has a classification accuracy rate of 90% for cervical adenocarcinoma tissue, 96.25% for cervical squamous cell carcinoma tissue and a total accuracy rate of 93.125%. The ROC curve was adopted to verify the

Table 2
Classification using the PCA–SVM algorithm.

A Style Polynomial	N (train)/N (test)	Adenocarcinoma	Squamous cell carcinoma	Total	Accuracy
Cervical adenocarcinoma	235/80	72	8	315	90%
Cervical squamous cell carcinoma	263/80	3	77	343	96.25%
B **Style line**	**N (train)/N (test)**	**Adenocarcinoma**	**Squamous cell carcinoma**	**Total**	**Accuracy**
Cervical adenocarcinoma	235/80	58	22	315	72.5%
Cervical squamous cell carcinoma	263/80	8	72	343	90%
C **Style Radial basis function**	**N (train)/N (test)**	**Adenocarcinoma**	**Squamous cell carcinoma**	**Total**	**Accuracy**
Cervical adenocarcinoma	235/80	52	28	315	65%
Cervical squamous cell carcinoma	263/80	9	71	343	88.75%
D **Style Sigmoid**	**N (train)/N (test)**	**Adenocarcinoma**	**Squamous cell carcinoma**	**Total**	**Accuracy**
Cervical adenocarcinoma	235/80	55	25	315	68.75%
Cervical squamous cell carcinoma	263/80	17	63	343	78.75%
E. Classification using the PCA-LDA algorithm					
Style LDA	**N (train)/N (test)**	**Adenocarcinoma**	**Squamous cell carcinoma**	**Total**	**Accuracy**
Cervical adenocarcinoma	235/80	78	2	315	97.5%
Cervical squamous cell carcinoma	263/80	70	10	343	12.5%

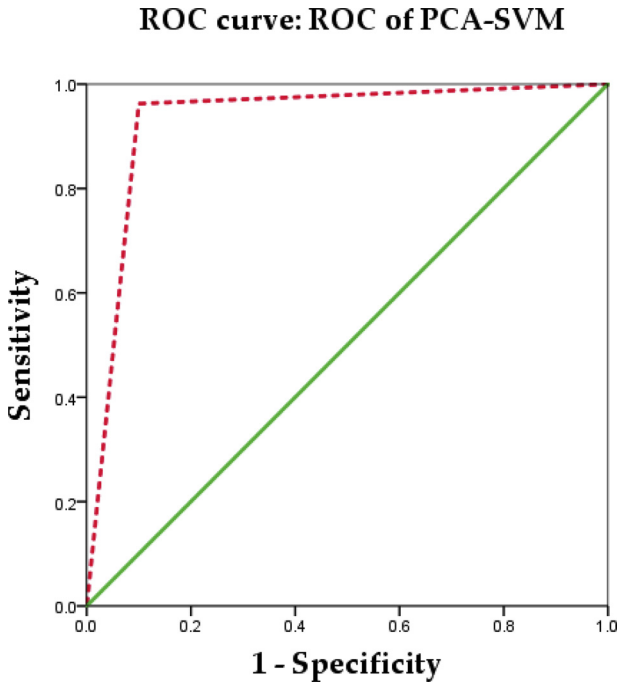

Fig. 4. ROC curve of the PCA–SVM model based on the polynomial kernel function.

reliability of the PCA-SVM classification model based on the polynomial kernel function, as shown in Fig. 4. The area under the ROC curve was 0.932, indicating that the model had high reliability.

In this study, the number of samples was limited, and we will continue to collect samples for future studies. We hope to establish a standard Raman spectroscopy library of cervical adenocarcinoma and cervical squamous cell carcinoma tissues with the support of a large number of samples and data.

In the future, we will further study Raman spectroscopy of different types of cervical tissues in detail. We hope to develop an endoscopic Raman spectroscopy detection system, which combines optical fibre technology with Raman spectroscopy technology and can be used for the clinical diagnosis of cervical cancer.

4. Conclusion

In this study, the normalized mean Raman spectra of cervical adenocarcinoma and cervical squamous cell carcinoma tissues were compared and analysed. The Raman intensity peaks at 640, 695, 838, 880, 1002, 1032, 1043, 1236, 1616, 1645 and 1670 cm^{-1}, attributed to proteins, at 614, 1095 and 1452 cm^{-1}, attributed to lipids, and at 485 and 898 cm^{-1}, attributed to glycogen, provided adequate differentiation between cervical adenocarcinoma and cervical squamous cell carcinoma tissues. The scatter plot of the relative intensity of all the spectra at 1002, 1340 and 1452 cm^{-1}, were drawn. The scatter plots were analysed in detail. The results showed that the relative intensity of the characteristic peaks at 1002, 1340 and 1452 cm^{-1} was significantly different ($P < 0.001$). The Raman spectroscopy combined with the PCA-SVM model was established for the classification of cervical adenocarcinoma and cervical squamous cell carcinoma tissues; the accuracy of the identification reached 93.125%.

This study indicated that there were significant differences in Raman spectrum between cervical adenocarcinoma tissues and cervical squamous cell carcinoma, and Raman spectroscopy combined with PCA-SVM could achieve the classification and differentiation of cervical adenocarcinoma and cervical squamous cell carcinoma.

Conflicts of interest

Authors have no conflicts of interest.

Acknowledgements

This work is supported by the Urumqi Science and Technology Project (No. P161310002), the National Science Foundation of China (No. 61765014), the Reserve Talents Project of the National High-level Personnel of Special Support Program (QN2016YX0324), and the Reserve National Youth Talent Support Program (Xinjiang[2014]22).

References

[1] F. Bray, J. Ferlay, I. Soerjomataram, R.L. Siegel, L.A. Torre, A. Jemal, Global cancer statistics 2018: GLOBOCAN estimates of incidence and mortality worldwide for 36 cancers in 185 countries, CA Cancer J. Clin. 68 (2018) 394–424.

[2] D. Cohn, Clinical practice guidelines in oncology: cervical cancer, J. Natl. Compr. Cancer Netw. 11 (2013) 320–343.

[3] T.P. Hanna, G.P. Delaney, M.B. Barton, The population benefit of radiotherapy for gynaecological cancer: local control and survival estimates, Radiother. Oncol. 120 (2016) 370–377.

[4] N. Rashid, H. Nawaz, K.W.C. Poon, F. Bonnier, S. Bakhiet, C. Martin, Raman microspectroscopy for the early detection of pre-malignant changes in cervical tissue, Exp. Mol. Pathol. 97 (2014) 554–564.

[5] S. Duraipandian, J.H. Mo, W. Zheng, Z.W. Huang, Near-infrared Raman spectroscopy for assessing biochemical changes of cervical tissue associated with pre-carcinogenic transformation, Analyst 139 (2014) 5379–5386.

[6] E. Vargis, E.M. Kanter, S.K. Majumder, M.D. Keller, R.B. Beaven, G.G. Rao, Effect of normal variations on disease classification of Raman spectra from cervical tissue, Analyst. 136 (2011) 2981.

[7] E.M. Kanter, S. Majumder, E. Vargis, A. Robichaux-Viehoever, G.J. Kanter, H. Shappell, H.W. Jones III, A. Mahadevan-Jansen, Multiclass discrimination of cervical precancers using Raman spectroscopy, J. Raman Spectrosc. 40 (2009) 205–211.

[8] K.L. Charlotte, A. Max, B. Hugh, W. James, H. Joanne, K. Catherine, Stone Nick, Advances in the clinical application of Raman spectroscopy for cancer diagnostics, Photodiagn. Photodyn. Ther. 10 (2013) 207–219.

[9] S. Duraipandian, W. Zheng, J. Ng, J.J.H. Low, A. Ilancheran, Z.W. Huang, In vivo diagnosis of cervical precancer using Raman spectroscopy and genetic algorithm techniques, Analyst 136 (2011) 4328–4336.

[10] P.R. Jess, D.D. Smith, M. Mazilu, K. Dholakia, A.C. Riches, C.S. Herrington, Early detection of cervical neoplasia by Raman spectroscopy, Int. J. Cancer 121 (2007) 2723–2728.

[11] D. Lin, S. Qiu, W. Huang, Autofluorescence and white light imaging-guided endoscopic Raman and diffuse reflectance spectroscopy for in vivo nasopharyngeal cancer detection, J. Biophotonics 11 (2018), https://doi.org/10.1002/jbio.201700251.

[12] E. Cordero, In-vivo Raman spectroscopy: from basics to applications, J. Biomed. Opt. 23 (2018) 1.

[13] F.M. Lyng, Vibrational spectroscopy for cervical cancer pathology, from biochemical analysis to diagnostic tool, Exp. Mol. Pathol. 82 (2007) 121–129.

[14] C.M. Krishna, N.B. Prathima, R. Malini, B.M. Vadhiraja, R.A. Bhatt, D.J. Fernandes, Raman spectroscopy studies for diagnosis of cancers in human uterine cervix, Vib. Spectrosc. 41 (2006) 136–141.

[15] M. Zanyar, R. Shazza, D.I. Rehman, Raman spectroscopy of biological tissues, Appl. Spectrosc. Rev. 42 (2007) 49.

[16] E.O. Faolain, M.B. Hunter, J.M. Byrne, P. Kelehan, M. McNamer, H.J. Byrne, F.M. Lyng, A study examining the effects of tissue processing on human tissue sections using vibrational spectroscopy, Vib. Spectrosc. 38 (2005) 121–127.

[17] W. Liu, H. Wang, J. Du, C. Jing, Raman microspectroscopy of nucleus and cytoplasm for human colon cancer diagnosis, Biosens. Bioelectron. 97 (2017) 70–74.

[18] R. Malini, K. Venkatakrishma, J. Kurien, Discrimination of normal, inflammatory, premalignant, and malignant oral tissue: a Raman spectroscopy study, Biopolymers 81 (2006) 179–193.

[19] Z. Huang, A. McWilliams, M. Lui, D.I. McLean, S. Lam, H. Zeng, Near-infrared Raman spectroscopy for optical diagnosis of lung cancer, Int. J. Cancer 107 (2003) 1047–1052.

[20] J. Zhao, H. Lui, D.I. Mclean, Automated autofluorescence background subtraction algorithm for biomedical Raman spectroscopy, Appl. Spectrosc. 61 (2007) 1225–1232.

[21] G. Shetty, C. Kedall, N. Shepherd, N. Stone, H. Barr, Raman spectroscopy: evaluation of biochemical changes in carcinogenesis of oesophagus, Br. J. Cancer 94 (2006) 1460–1464.

[22] J.W. Chan, D.S. Taylor, T. Zwerdling, S.T. Lane, K. Ihara, T. Huser, Micro-Raman spectroscopy detects individual neoplastic and normal hematopoietic cells, Biophys. J. 90 (2006) 648–656.

[23] C.J. Frank, R.L. McCreecy, D.C.B. Redd, Raman spectroscopy of normal and diseased human breast tissues, Anal. Chem. 67 (1995) 777–783.

[24] N. Kokolis, I. Ziegler, On the levels of phenylalanine, tyrosine and tetrahydrobiopterin in the blood of tumor-bearing organisms, Cancer Biochem. Biophys. 2 (1977) 79–85.

[25] M.N. Harvie, I.T. Campbell, A. Howell, N. Thatcher, Acceptability and tolerance of a low tyrosine and phenylalanine diet in patients with advanced cancer—a pilot study, J. Hum. Nutr. Diet. 15 (2002) 10.

[26] G. Gueron, P. Anselmino, Nicolás Chiarella, E.G. Ortiz, S. Lage Vickers, A.V. Paez, Game-changing restraint of ros-damaged phenylalanine, upon tumor metastasis, Cell Death Dis. 9 (2018) 140.

[27] S. Samnick, B.F.M. Romeike, B. Kubuschok, P-[123I]iodo-l-phenylalanine for detection of pancreatic cancer: basic investigations of the uptake characteristics in primary human pancreatic tumour cells and evaluation in in vivo models of human pancreatic adenocarcinoma, Eur. J. Nucl. Med. Mol. Imaging 31 (2004) 532–541.

[28] R.K. Dukor, Vibrational spectroscopy in the detection of cancer, Biomed. Appl. 5 (2002) 3335–3359.

[29] B. Yan, Y. Li, G. Yang, Z.N. Wen, M.L. Li, L.J. Li, Discrimination of parotid neoplasms from the normal parotid gland by use of Raman spectroscopy and support vector machine, Oral Oncol. 47 (2011) 430–435.